# Machining effects on damage evolution in sinter powder metals

**S. Ma, H. Yuan***

Department of Mech. Engineering, University of Wuppertal, Wuppertal 42119, Germany
* Corresponding author: h.yuan@uni-wuppertal.de

**Abstract** The sinter powder metals have found extensive engineering applications in industry. The mechanical property of sinter metals is characterized by high porosity and micro-cracks. Inelastic behavior of the materials is coupled with micro-crack propagation and coalescence of open voids. The machining of sinter metals has significant influence on material behavior. In the present paper the machining effect on damage evolution of sinter iron is investigated under tension and torsion loading conditions experimentally and computationally. The tests indicated that damage of the sinter iron initiated already at a stress level much lower than the macroscopic yield stress. Based on the uniaxial tensile test an elastic-plastic continuum damage model was developed which predicts influence of machining on the damage evolution in the sinter iron under tension and torsion loading conditions. The proposed damage model can reasonably predict the damage evolution under tension loading for sintered iron. Deviation to the torsion damage is significant which implies anisotropic damage evolution.

**Keywords** Sintered metal, continuum damage model, damage evolution, machining effects

## 1. Introduction

Powder metallurgy (PM) technology has many advantages in comparison with melting metallurgy technology, e.g. low manufacturing cost, high production efficiency, high precision geometry and flexible composition of metal elements. With development of powder metallurgy technology many high performance components working under high and complex loading conditions are made of PM steel in recent years. Microstructure of sintered metals is characterized by high porosity and micro-cracks. Inelastic behavior of the material is coupled with inelastic deformations of powder particles, micro-crack propagation and coalescence of voids [6]. Interconnected porosity may cause higher stress concentrations near the particle connecting necks, while isolated porosity results in more homogeneous deformations [13]. Microscopic damage mechanism of sintered metals is investigated in monotonic in-situ tensile tests [3]. It is found that micro-cracks always initiate at pores of which the long axis is perpendicular to the tensile axis. These micro-cracks open and/or propagate under the mode I crack direction. Additional effects on material property are related to machining of sinter materials [13]. Experimental observations confirm that both mass density and elasticity modulus are significantly changed due to turning manufacture. A dramatic drop is determined in the fracture strain, which decreases from 14% to 3-4%, as reported in [13]. It is of importance to quantify effects of machining in mechanical property of sinter metal parts.

In the present work, damage from machining is studied experimentally and computationally. The damage evolution in specimens fabricated in two different machining processes is investigated under tension and torsion loading conditions. The damage variable is defined within the framework of thermodynamics and experimentally determined by monitoring changes of Young's modulus or shear modulus. It is found that damage in the sintered iron nucleates at a load level much lower than yield stress and fractured in the semi-brittle manner in spite of large plastic deformations. The machining effects on the mechanical properties were experimentally quantified and represented as state variable in the proposed continuum damage model. The continuum damage model should be able to predict the damage evolution in the sintered iron and verified based on detailed experiments. The influence of machining on the damage evolution was predicted with the proposed damage model, where the initial damage duo to machining is considered.

## 2. Materials and Specimen fabrication

To investigate mechanical behavior of sinter metals, the pure iron powder (atomized Hoeganaes ASC.100.29) from Hoeganaes Corporation was used to produce specimens. The organic binder (0.6% HDL-wax) is added into iron powder to improve lubricity during compaction of the green material. The green material is sintered at 1120°C for 60 min in the 95% $N_2$ and 5% $H_2$ atmosphere. The binder was burned out in the first stage of sintering. The average density of material after sintering is 7.2g/cm3, that is, the material contains ca. 8% air, i.e. porosity. The tensile bars specimens (Fig. 1) are fabricated directly by compacting and sintering, which is considered as reference material to determine machining effect on mechanical properties of material. The tubular specimens (Fig. 2), however, cannot be sintered directly and have to be machined from large piece of sinter materials. In the present work, the tubular parts are taken from cylindrical blanks with a diameter of 200mm. Generally speaking, the material property of the sinter iron is very sensitive to machining process.

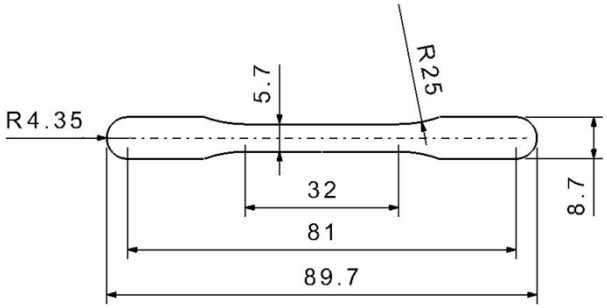


**Figure 1**. MPA specimen without machining

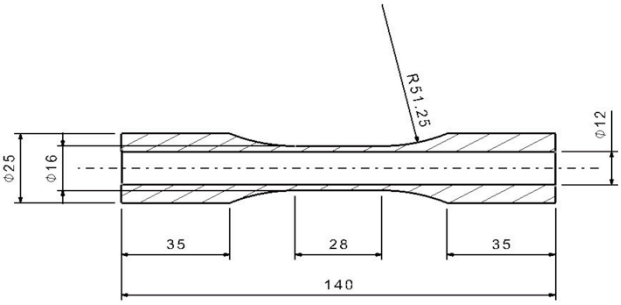


**Figure 2**. Thin-walled tube specimen by machining

The tubular specimens were machined with two different fabrication procedures in order to investigate the influence of machining procedure. The first procedure is followed by a conventional mechanical machining procedure of tubular specimen: Drilling-boring-turning (TBD). In this machining procedure the machining speed was well controlled. With the second machining method, the hole of the tubular specimen was mainly fabricated with the wire cut electrical discharge machining (WEDM) technology. After wire cutting, the remained thin oxide layer was removed by grinding. In compare with conventional machining procedures, the second fabrication procedure is more time-consuming.

## 3. Experimental results

### 3.1. Machining effect on the stress-strain curve

For investigating the effect of machining on mechanical properties of sintered iron, tensile tests were carried out with both tensile bar specimens und tubular specimens fabricated by different machining procedures. The tensile bar specimen is as-sintered without additional machining, which is the reference specimen for tension test of sintered steel according to DIN EN ISO 2740. In Fig. 3, it is shown that the tensile bar specimen shows a distinct Lüder's band, whereas it was not observed in the tubular specimen fabricated by TBD. The machining induces severe plastic deformations into specimen and the material seems strong to be hardened due to cold-working. The Lüder's band disappear in the TBD tubular specimen. With WEDM the tubular specimen seems not much different and its stress-strain curve nearly coincides with that of the tensile bar specimen (Fig 3). The most dramatic change due to machining is observed in the fracture strain, whereas the tensile bar specimen was broken at 12-14% of elongation, the TBD specimen shows 3.8% as fracture strain. More mechanical properties of both as-sintered and machined specimens are summarized in Table 1. Whereas WEDM does not distort sinter material, TBD generates significant damage to the specimen. Damage from conventional machining can affect sinter metal property substantially.

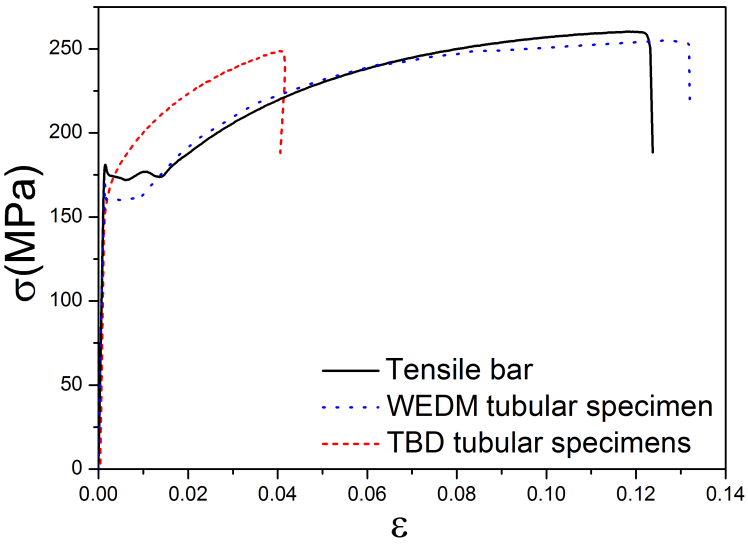


**Figure 3**. Stress-strain curves from differently fabricated specimens.

The porosity of specimens was measured before and after conventional machining by image analysis technique and Archimedes method, respectively. Optical micrographs revealed a significant increase of porosity after TBD machining. The average density of specimens after machining was increased from 7.2g/cm$^3$ to 7.4g/cm3, which is higher than the density before machining. In other words, the porosity of specimen before machining was reduced from 8.5% to 6% after machining procedure (TBD). The material of specimen was densified during machining.

**Table 1.** Mechanical properties of tensile specimen and tubular specimens.

| Specimen Type | E [GPa] | $\sigma_y$ [MPa] | $\sigma_u$ [MPa] | $\varepsilon_f$ [%] |
|---|---|---|---|---|
| Tensile bar without machining | 164 | 135 | 255 | 12.3 |
| Tubular specimen (TBD) | 163 | 130 | 248 | 3.8 |
| Tubular specimen (WEDM) | 162 | 134 | 254 | 12.7 |

For sintered metal, Young's modulus can be expressed as a function of the porosity of material

$$\frac{E}{E_{ful}} = (\frac{\rho}{\rho_{ful}})^{\omega}, \tag{1}$$

where $\rho$ is the porosity of material, $\rho_{ful}$ is density of fully dense material ($\rho_{ful}$=7.86g/cm$^3$ for iron), and $E_{ful}$ is the Young's modulus of fully dense material (according to literature the Young's modulus of fully dense iron is 201GPa) [3]. With the elastic modulus of specimen for density 7.2 g/cm$^3$, one obtains that $\omega$=2.46. For the material of density 7.4 g/cm$^3$ the theoretical elastic modulus should be 176GPa. Compared with elastic modulus determined in the experiment, it implies that the specimen contains initial damage after conventional machining, which reduces the elastic modulus.

Summarizing observations above, one may conclude that the conventional machining procedure will harden and embrittle the sintered iron significantly. Furthermore, the material is densified and damaged during machining. With the WEDM machining, the machining effect is insignificant. The material properties of as-sintered material can be approximated by the WEDM

tubular specimen.

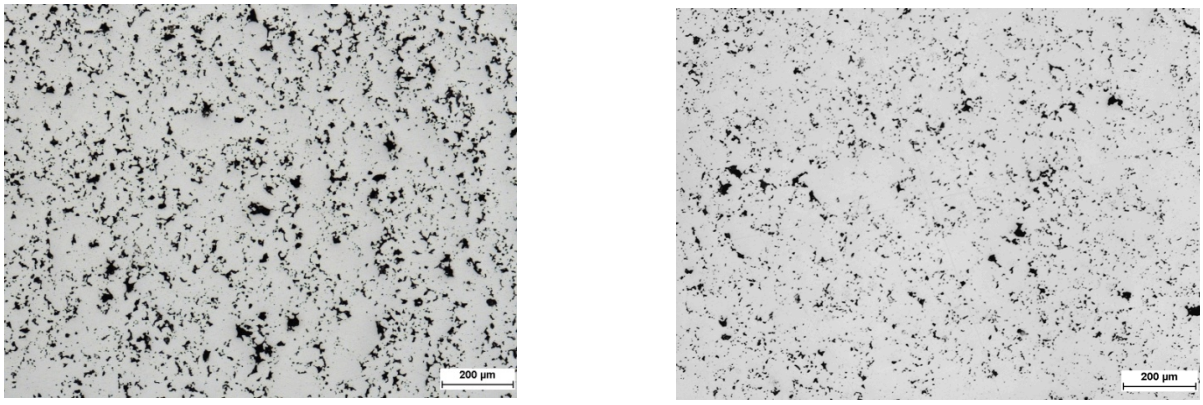


(a) (b)

**Figure 5.** Microstructures of the sintered iron ASC.100.29 with density 7.2g/cm$^3$. (a) Before machining. (b) After conventional machining (TBD) the material is densified to 7.4g/cm$^3$.

### 3.2. Damage evolution in different specimens

The loading and unloading cycles were designed to accomplish in different loading stage in order to investigate the damage evolution in the whole loading range. All tests were performed at a strain rate about $10^{-4}$/s and at room temperature in MTS 809 axial/torsion testing machine. Axial/torsional extensometer of MTS Corp. was used to measure axial and torsional strains during tests. The gauge length of the extensometer used was 25mm.

Material damage can be expressed by diminishing of the elastic modulus [10],

$$D = 1 - \frac{E(\epsilon)}{E_0} \tag{2}$$

where $E_0$ denotes the initial elasticity modulus of the sintered metal without damage and $E$ depending on deformations stands for actual elasticity modulus. With developing material damage, the material stiffness, i.e. $E$-modulus, decreases. In experiments $E$ is determined from unloading controlled by stress to avoid compression according to the suggestion of Lemaitre [10], as shown in Fig. 6(a). Since unloading is limited within a small range, damage due to unloading is negligible.

The damage evolution in the uniaxial tension test is plotted in Fig. 6(b). In the figure the damage evolutions of tensile bar and WEDM tubular specimen are nearly identical. That is, the WEDM machining has negligible influence on the damage evolution. On the other side, the material stiffness loses dramatically in very small strain and then diminishes almost linearly. This result implies that material damage nucleates even under elastic loading condition and develops with further inelastic strains. The relation between damage and stress/strain can be approximated by the known Ramberg-Osgood model, as

$$D = A\sigma + B\epsilon^m \tag{3}$$

with $A$, $B$ and $m$>1 as fitting parameters. The damage relation in Eq. (3) is shown in Fig. 6(b) and its development is dominated by the linear term in small loading region. Damage is nucleated under elastic material state and mainly linear proportional to applied stress, since the nonlinear term is vanishingly small for small strain. If the material becomes plastic, the strain will grow over-proportionally, so that the influence of the linear term disappears. The exponent $m$ is larger than 1, so that the damage curve for the sintered metals is convex. From dense ductile materials it is known that damage nucleates at large plastic strain and grows very gradually, the damage evolution curve is concave [10]. The convex development implies a very different damage mechanism in the

sintered metal.

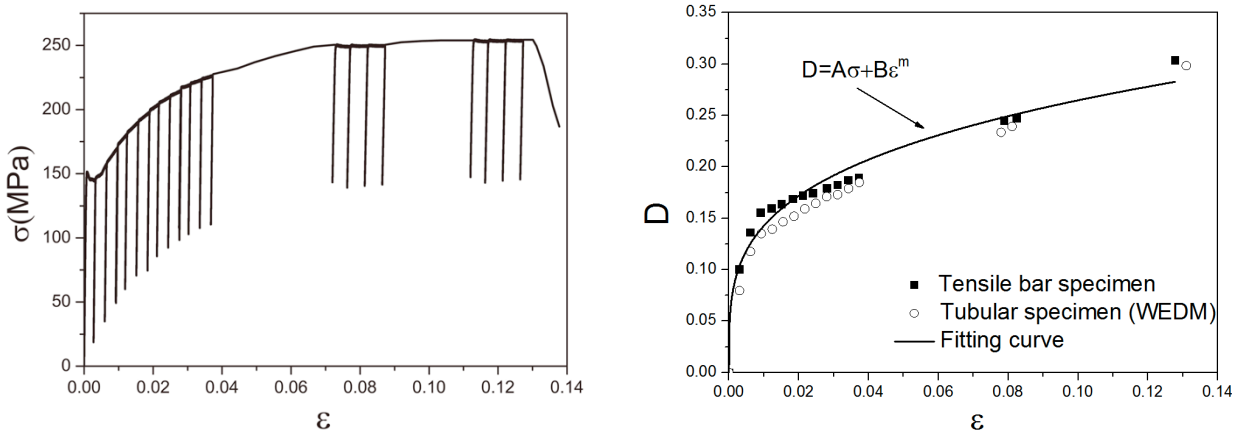


**Figure 6.** Uniaxial tensile tests. (a) Loading-unloading cycle to determine elastic modulus. (b) Damage as a function of strain.

Damage evolution in torsion can be determined in the same way as that in tension. The influence of machining on damage evolution is shown in Fig. 7 for both tension and torsion loadings, where damage is expressed as a function of the equivalent strain, $\varepsilon_{eq} = \sqrt{\varepsilon^2 + \gamma^2/3}$. The experiments reveal that the damage evolution under shearing is similar to that under tension. But the fracture strain of torsion is dramatically larger than that from tension, which implies effects of the stress triaxiality. As expected, damage in the TBD specimens develops more quickly than that in the WEDM specimens and the TBD specimens fail at smaller strains for both tension and torsion loadings. But the influence of machining on the damage evolution under torsion loading is smaller than under tension.

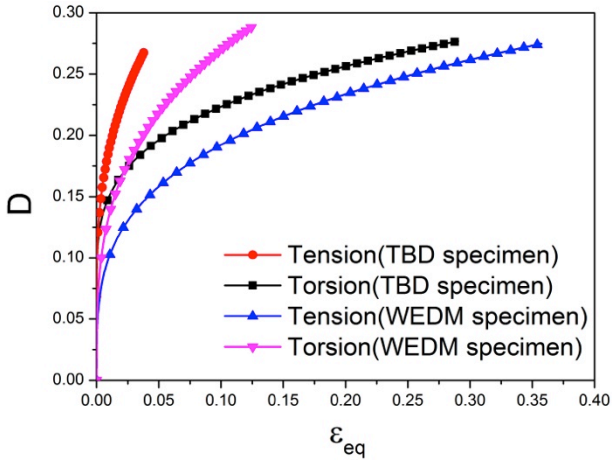


**Figure 7.** Evolutions of damage in different specimens.

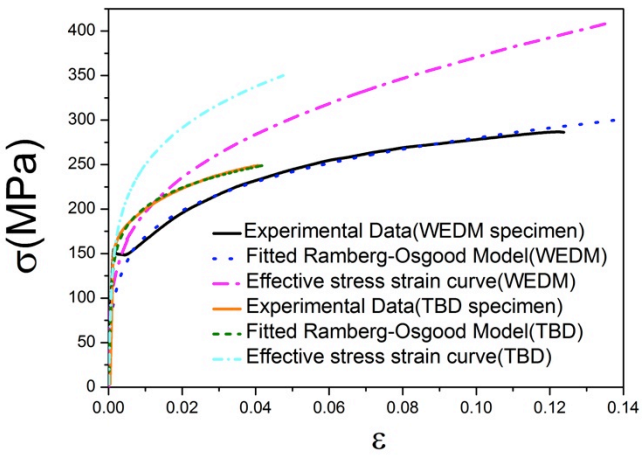


**Figure 8**. Effective stress-strain curves

## 4. Continuum damage model

In the framework of infinitesimal deformation, the strain rate tensor is decomposed into elastic and plastic part as

$$\dot{\epsilon}_{ij} = \dot{\epsilon}^e_{ij} + \dot{\epsilon}^p_{ij}. \tag{4}$$

In the present work, the scalar damage variable as defined in (1) is introduced to describe degradation of the sintered metal in the framework of continuum damage mechanics. Based on the strain equivalence hypothesis, the effective stress in the undamaged configuration is defined as [1,2,10]

$$\tilde{\sigma}_{ij} = \frac{\sigma_{ij}}{(1-D)}. \tag{5}$$

The effective stress-strain curves for both types of specimens are plotted in Fig. 8. Then, the thermodynamic driving force associated with damage variable $D$ is given based on the thermodynamic framework for continuum damage model proposed by Lemaitre [8,10] as

$$Y = \frac{\sigma_e^2}{2E_0(1-D)^2} f(\eta), \tag{6}$$

with

$$f(\eta) = \frac{2}{3}(1+\nu) + 3(1-2\nu)\eta^2. \tag{7}$$

Above $f(\eta)$ represents dependence on the stress triaxiality, $\eta = \sigma_H / \sigma_{eq}$, where $\sigma_H$ is the hydrostatic stress and $\sigma_{eq}$ is Mises stress.

### 4.1. The damage evolution law with initial damage

Experimental observations for the sintered metals reported in the previous section reveal that material damage occurs under very low stress amplitude, i.e. damage is induced by elastic deformations before the material is plastic. Thus, the damage variable can be decomposed into elastic damage and plastic damage, as

$$D = D^e + D^p. \tag{8}$$

Obviously, the decomposition is consistent to experimental data for the uniaxial state, Eq. (3).

#### *4.1.1. Elastic damage evolution*

The elastic damage was known in brittle materials, such as concrete, rocks etc. Various elastic CDM models have been developed for modeling elastic damage accumulation in the brittle materials [7，9], which can be extended to characterize the elastic damage in the sintered metal. The potential function for the elastic damage is defined as

$$F_e^D = Y - Z(D_e), \tag{9}$$

where Z is the material resistance against material damage. Following the material resistance can be expressed in the exponential form

$$Z = Y_0 + \frac{1}{b}\ln\left(\frac{D_e^{sa} - D_e^0}{D_e^{sa} - D_e}\right), \tag{10}$$

where $Y_0$ is the initial resistance against material damage and $b$ is a model parameter. $D_e^{sa}$ represents the saturation of the elastic damage since in elastic-plastic materials the elastic damage will not finally destroy the structure but accelerate the final failure. $D_e^0$ denotes initial elastic damage, which can be induced by manufacturing process or previous loading history. From the maximum dissipation principle, the damage evolution law is expressed in the rate-form as

$$\dot{D}_e = \dot{\lambda}_b \frac{\partial F_e^D}{\partial Y} = \dot{\lambda}_b. \tag{11}$$

In case with damaging, the damage multiplier $\dot{\lambda}_b$ is determined by the damage consistency condition,

$$dF_e^D = \frac{\partial F_e^D}{\partial Y}\dot{Y} - \frac{\partial Z}{\partial D_e}\dot{\lambda}_b = 0. \tag{12}$$

The evolution equation of the elastic damage is expressed as

$$\dot{D}_e = (D_e^{sa} - D_e^0)\, b \exp\left[-b\left\langle Y - Y_0 \right\rangle\right]\dot{Y}, \tag{13}$$

or

$$D_e = D_e^0 + (D_e^{sa} - D_e^0)\left\{1 - \exp\left[-b\left\langle Y - Y_0 \right\rangle\right]\right\}. \tag{14}$$

where $\left\langle \cdot \right\rangle$ is the Macauley bracket, i.e. $\left\langle x \right\rangle = \left(|x| + x\right)/2$.

*4.1.2 Plastic damage evolution*

In ductile materials the damage is mainly accumulated due to plastic deformations. Following the concept by Bonora et al. [1, 2] interactions between plastic dissipation and damage dissipation can be neglected. The plastic damage dissipation potential $F$ exists and can be expressed as sum of plastic damage potential, $F_p^D$, and plastic deformation potential, $\Psi_p$, as

$$F = F_p^D + \psi_p. \tag{15}$$

Based on the hypothesis of the strain equivalence and the effective stress concept, the plastic dissipation potential for the material can take the form of the $J_2$ plasticity theory,

$$\psi_p = \tilde{\sigma}_e - \tilde{\sigma}_{y0} - R(r), \tag{16}$$

where the effective Mises stress is defined as

$$\tilde{\sigma}_e = \sqrt{\frac{3}{2}\left(\frac{s_{ij}}{1-D}\right)\left(\frac{s_{ij}}{1-D}\right)} \tag{17}$$

with $s_{ij}$ as the deviatoric stress tensor. The damage dissipation potential proposed after Bonora et al. [1, 2] for the plastic damage model is written as

$$F_p^D = \left[\frac{1}{2}\frac{Y^2}{S_0}\frac{1}{1-D}\right]\frac{(D_{cr}^p - D_p)^{(\alpha-1)/\alpha}}{p^{(2+n)/n}}, \tag{18}$$

where $S_0$ is damage material parameter, $n$ is the plastic hardening exponent in the Ramberg-Osgood model, $\alpha$ is the damage exponent that determines the shape of the damage evolution law and $p$ is the accumulated plastic strain. $D_p^{cr}$ is critical plastic damage value.

Based on the maximum dissipation principle, the evolution of internal variables can be obtained via the normality rule as

$$\dot{\epsilon}_{ij}^p = \dot{\lambda}_p \frac{\partial F}{\partial \sigma_{ij}} = \dot{\lambda}_p \frac{\partial \psi_p}{\partial \sigma_{ij}}, \dot{D}_p = \dot{\lambda}_p \frac{\partial F}{\partial Y} = \dot{\lambda}_p \frac{\partial F_p^D}{\partial Y}, \dot{\lambda}_p = \dot{p}(1-D). \tag{19}$$

The effective stress can be formulated as a function of the plastic strain in the Ramberg-Osgood law,

$$\tilde{\sigma}_{eq} = \frac{\sigma_{eq}}{1-D} = Kp^{1/n}. \tag{20}$$

Recalling Eqs. (18) - (20) and Eq. (6), the plastic damage evolution law is derived as

$$\dot{D}_p = \begin{cases} 0 & \text{if } p < \epsilon_{th} \text{ or } \sigma_H \le 0), \\ \dfrac{K^2}{2E_0 S_0} f(\eta) \left( \dfrac{(D_p^{cr} - D_p)^{(\alpha-1)/\alpha}}{p} \right) \dot{p} & \text{if } p \ge \epsilon_{th} \text{and } \sigma_H \ge 0). \end{cases} \tag{21}$$

It is assumed that the plastic damage will not grow in the compression stress state [2]. The plastic damage process remains inactive until the effective accumulated plastic strain $p$ reaches the threshold strain $\epsilon_{th}$ for the positive hydrostatic stress.

With $D_p = D_p^{cr}$ at $p = p_{cr}$ as the final critical damage to fracture, integrating the equation above over $[D_p^0, D_p^{cr}]$ for $D$ and $[\epsilon_{th}, p_{cr}]$ for $p$ under proportional loading condition, where $D_p^0$ is initial plastic damage, one gets

$$[D_p^{cr} - D_p^0]^{1/\alpha} = \frac{1}{\alpha} \frac{K^2}{2E_0 S_0} f(\eta) \ln\left( \frac{p_{cr}}{\epsilon_{th}} \right). \tag{22}$$

Integrating the equation above over $[D, D_p^{cr}]$ for $D$ and $[p, \epsilon_{cr}]$ for $p$, one gets

$$[D_p^{cr} - D^p]^{1/\alpha} = \frac{1}{\alpha} \frac{K^2}{2E_0 S_0} f(\eta) \ln\left( \frac{p_{cr}}{p} \right). \tag{23}$$

For uniaxial tension $f(\eta) = 1, p_{cr} = \varepsilon_{cr}$, Eq. (23) can be re-written into

$$[D_p^{cr} - D_p^0]^{1/\alpha} = \frac{1}{\alpha} \frac{K^2}{2E_0 S_0} \ln\left( \frac{\varepsilon_{cr}}{\epsilon_{th}} \right). \tag{24}$$

Dividing Eq. (24) with Eq. (23), one obtains the explicit expression for plastic damage as a function of the equivalent plastic strain for proportional loading cases

$$D_p = D_p^0 + (D_p^{cr} - D_p^0) \left\{ 1 - \left[ 1 - \frac{\ln(p/\epsilon_{th})}{\ln(\epsilon_{cr}/\epsilon_{th})} f(\eta) \right]^{\alpha} \right\}. \tag{25}$$

Dividing Eq. (23) by Eq. (25), the fracture strain under proportional loading can be expressed as

$$p_{cr} = \epsilon_{th} \cdot \left( \frac{\varepsilon_{cr}}{\epsilon_{th}} \right)^{1/[f(\eta)]} \tag{26}$$

### 4.2. Identification of model parameters

Identification of the damage model parameters is accomplished with uniaxial tests using the WEDM tubular specimens, i.e. tensile and compressive tests. For verification, the fracture strain in multi-axial experiments and influence of machining on the damage evolution of specimen should be predicted by the CDM [11].

In Fig. 8, the material parameters for Ramberg-Osgood power law can be obtained by fitting for both machining procedures. According to the experimental results, the average density of material is increased after machining. On the other words, the material is compressed during machining. It is well known that ductile damage grows more slowly in compression stress state. The initial plastic damage is negligible. The initial damage is considered as elastic damage. And the initial plastic damage is not activated during machining, $D_p^0 = 0$. The initial elastic damage is calculated by $D_e^0 = 0.074$, $E_0$ is 176GPa for material with density 7.4g/cm$^3$.

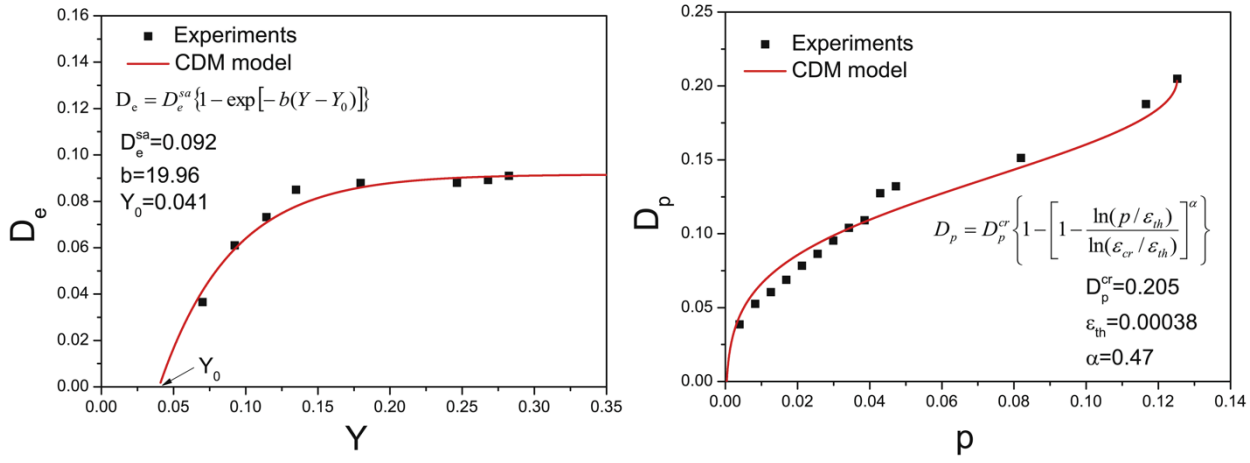


(a) (b)

**Figure** 9. Development of the damage as a function of applied load. Symbols denote experimental data and curves are results from the CDM model. (a) Evolution of the elastic damage with energy release rate. (b) Plastic damage evolution with the plastic strain.

Since it is assumed that plastic damage will not accumulate in the compressive stress state, the compression test is used to identify the model parameters of the elastic damage evolution for the isotropic elastic damage. The elastic damage becomes almost stationary for higher loading. The model parameters $D_e^{sa}$, $b$ and $Y_0$ are identified by fitting the experimental curve as shown in Fig 9(a).

The plastic damage evolution should be obtained from the elastic-plastic tensile tests. From the uniaxial tensile tests the critical ductile damage can be approximated by $D_p^{cr} = D_{cr} - D_e^{sa}$. The result of Eq. (25) is plotted in Fig. 9(b), in which the ductile damage is expressed as a function of the plastic strain. The material parameters of the elastic-ductile damage model for sintered iron are summarized in Table 2.

**Table 2.** Summary of the material model parameters for the sintered iron

| |
|---|
| Elasto-plastic material properties: |
| Tubular specimen(Conventional machining) |
| $E_0$ = 176000MPa; ν = 0.27; $\sigma_{y0}$ = 135MPa; n = 4.955; K = 608MPa |
| Tubular specimen(WEDM) |
| $E_0$ = 162000MPa; ν = 0.27; $\sigma_{y0}$ = 135MPa; n = 4.714; K = 549MPa |
| Elastic damage evolution law: |
| $D_b^{sa}$ = 0.091; b = 19.961; $Y_0$ = 0.04MPa, |
| Plastic Bonora damage evolution law: |
| $\epsilon_{th}$ = 0.00038; α = 0.47; $S_0$ = 27.85MPa; $\epsilon_{cr}$ = 0.12522; $D_p^{cr}$ = 0.205; $D^{cr}$ = 0.296 |

### 4.3. Failure Prediction of the CDM model

Using the material parameters identified in the previous section, damage evolution of sintered iron is predicted for both tension and torsion loading condition according to Eq. (25). Furthermore, the equivalent fracture strain is also predicted for combined tension-torsion condition with Eq. (26).

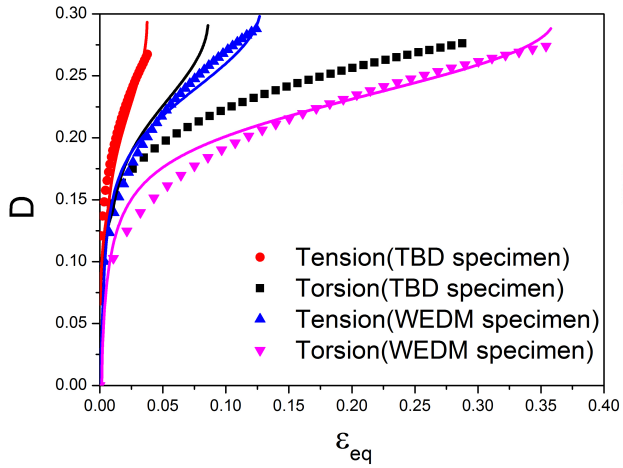


**Figure** 10. Comparison between experiments and computational predictions

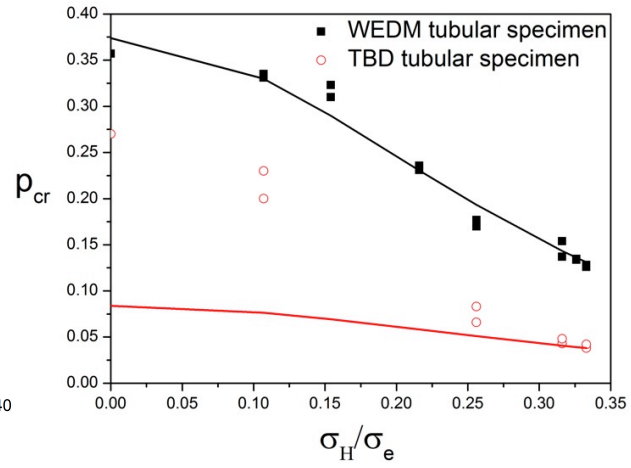


**Figure** 11. Variations of final fracture strain in tension-torsion specimens.

Experimental observations of different sinter metal specimens are plotted in Figs. 10 and 11 in which symbols denote experimental data. With increasing stress triaxiality, the material behaves more brittle, that is, the fracture strain decreases rapidly. Obviously, the prediction from the CDM model is accurate for the WEDM specimens in comparison with the tension and torsion tests.

For the TBD specimen, it is seen that the proposed model is not able to accurately predict the machining effect on the damage evolution under torsion loading. The deviation becomes more significant with decreasing stress triaxiality in the range of $\eta < 0.25$. That means that the machining influence on the damage evolution is strongly depending on loading mode. In the machining process, the initial damage induced by mainly shearing in specimen. Under this situation the damage in the form of micro-cracks would be perpendicular to the specimen axis, which is very sensitive to axial tension, not to the torsion. That is, the damage is strongly anisotropic. Additionally, the initial damage is not constant in the tubular specimen. It will lead to stress gradient in the subsurface of specimen. For this reason, the initial damage gradient has to be considered in investigation of machining effect in order to reasonably predict the damage evolution of material contains machining effect.

## 5. Conclusions

In the present work damage evolution in a sinter iron is studied experimentally and computationally. Based on both analytical and computational discussions following conclusions can be drawn:

- Experiments on both tension and torsion tests confirm that the sinter material stiffness decreases rapidly with applied load. The degradation of material occurs at much lower load level than yield stress.
- The damage variable in the continuum damage model is decomposed into elastic damage and plastic damage, where the elastic damage is characterized by the stress and the plastic damage is mainly controlled by the plastic strain. The evolution equations for both damage variables have been developed within the framework of thermodynamics. The initial damage is considered in the damage evolution law. Explicit expressions for both damage evolutions have been obtained.
- Conventional machining (TBD) has significant influence on the mechanical properties of the

sintered iron. The sinter metal is densified，hardened and damaged. Fracture strain decreases dramatically. The machining changes the dependence of damage evolution on loading mode. The results show that the proposed damage model is able to predict machining influence on damage evolution under tension loading, but not under torsion.

**References**

[1] N. Bonora. A nonlinear CDM model for ductile failure. Engineering Fracture Mechanics 58 (1) (1997) 11–28.
[2] N. Bonora, D. Gentile, a. Pirondi, G. Newaz. Ductile damage evolution under triaxial state of stress: theory and experiments. International Journal of Plasticity 21 (5) (2005) 981–1007.
[3] S. Carabajar, C. Verdu, R. Fougeres. Damage mechanisms of a nickel alloyed sintered steel during tensile tests. Materials Science and Engineering: A 232 (1-2) (1997) 80–87.
[4] J. L. Chaboche, M. Boudifa, K. Saanouni. A CDM approach of ductile damage with plastic compressibility. International Journal of Fracture 137 (1-4) (2006) 51–75.
[5] N. Chawla, B. Jester, D. Vonk. Bauschinger effect in porous sintered steels. Materials Science and Engineering: A 346 (1-2) (2003) 266–272.
[6] J. Chen, H. Yuan, M. Schneider. Investigation of micromechanical deformation mechanisms in sinter powder metals. Advanced Material Research, in print.
[7] U. Cicekli, G. Z. Voyiadjis, and R. K. Abu Al-Rub. A plasticity and anisotropic damage model for plain concrete, International Journal of Plasticity 23 (10-1) (2007) 1874–1900.
[8] R. Desmorat, S. Cantournet. Modeling microdefects closure effect with isotropic/anisotropic damage. International Journal of Damage Mechanics 17 (1) (2007) 65–96.
[9] O. Kintzel, S. Khan, J. Mosler. A novel isotropic quasi-brittle damage model applied to LCF analyses of Al2024. International Journal of Fatigue 32 (12) (2010) 1948–1959.
[10] J. Lemaitre, R. Desmorat. Engineering damage mechanics: Ductile, creep, fatigue and brittle failures, Springer-Verlag, 2005.
[11] S. Ma, H. Yuan. Damage evolution and modeling of sinter metals under multi-axial loading conditions. Computational Materials Science, submitted for publication.
[12] X. Pan, H. Yuan. Computational algorithms and applications of element-free Galerkin methods for nonlocal damage models. Engineering Fracture Mechanics 77 (2010), 2640-2653
[13] M. Schneider, H. Yuan. Experimental and computational investigation of cyclic mechanical behavior of sintered iron. Computational Materials Science 57 (2012) 48 – 58.
[14] C. M. Sonsino. Zukunftsperspektiven für die Pulvermetallurgie durch die Betriebsfestigkeit. Materialwissenschaft und Werkstofftechnik 37 (3) (2006) 240–248.
[15] H. Yuan, J. Chen, K. Krompholz, F.H. Wittmann. Investigations of size effects in tensile tests based on a nonlocal micromechanical damage model. Computational Materials Science 26 (2003) 230-243